Genomics Communications

ARTICLE

Open Access

https://doi.org/10.48130/gcomm-0025-0020

Genomics Communications **2025**, 2: e020

Evolutionary conservation of *YTH domain-containing* genes facilitating the functional achievement of m^{6}A-modified RNAs under abiotic and biotic stresses in spotted sea bass (*Lateolabrax maculatus*)

Huanhuan Zhu[1], Han Yu[1], Yun Li[1], Haishen Wen[1], Xin Qi[1], Boyuan Wang[2], Yuan Yao[3], Ye Lu[1], Jiahao Zhang[1], Cong Yan[1], Qinfeng Gao[1*] and Yuan Tian[1*]

[1] *Key Laboratory of Mariculture, Ministry of Education, Ocean University of China, Qingdao 266003, China*
[2] *Department of Biological Sciences, Auburn University, Auburn 36849-5412, USA*
[3] *Molecular Bioscience-Genetics and Genomics, Duke Kunshan University, Kunshan 215316, China*
* Corresponding authors, E-mail: qfgao@ouc.edu.cn; tianyuan@ouc.edu.cn

Abstract

YT521-B homology (YTH) domain-containing genes encode key reader proteins with the ability to recognize N^6-methyladenosine (m^{6}A) and mediate m^{6}A-related biological functions. Despite their importance, *YTH domain-containing* genes have not been systematically investigated in the vast majority of teleosts. In the present study, six *LmYTH* genes were identified in spotted sea bass through homologous alignment and a conserved domain search. Comparative analysis revealed high similarity in gene structures, the YTH domain's distribution, and motif sites in homologous *YTH domain-containing* genes between mouse and spotted sea bass. Through a three-dimensional structural analysis of YTH domain-containing proteins between mouse and spotted sea bass, similarities were found in the α-helixes and β-strands components, identical tryptophan–tryptophan–tryptophan- or tryptophan–tryptophan–leucine-type aromatic cages for m^{6}A recognition, and shared hydrogen bond formation. These results strongly supported the evolutionary conservation of *YTH domain-containing* genes between mammals and teleosts. RNA-seq datasets, together with quantitative real-time polymerase chain reaction experiments, revealed significant differences in the expression patterns of *LmDF1a*, *LmDF1b*, *LmDF3*, *LmDC1*, and *LmDC2*, implying their roles in response to abiotic and biotic stresses. Interestingly, *LmDF1a* and *LmDF1b*, a pair of duplicated genes, exhibited the opposite expression patterns, suggesting their potential function divergence in evolution. The present study offers a comprehensive perspective on *LmYTH* genes, unveiling their potential significance in response to abiotic and biotic stresses.

Citation: Zhu H, Yu H, Li Y, Wen H, Qi X, et al. 2025. Evolutionary conservation of *YTH domain-containing* genes facilitating the functional achievement of m^{6}A-modified RNAs under abiotic and biotic stresses in spotted sea bass (*Lateolabrax maculatus*). *Genomics Communications* 2: e020 https://doi.org/10.48130/gcomm-0025-0020

Introduction

N^6-methyladenosine (m^{6}A), the predominant methylation modification in RNAs, is crucial for various physiological and pathological processes in organisms[1,2]. This m^{6}A methylation was initially discovered in bacterial DNA in 1955, and then identified in mRNAs of mammalian cells during the early 1970s[3–5]. Recently, newly emerging methods have revealed a wide landscape of m^{6}A modifications in mRNAs, such as methylated RNA immunoprecipitation sequencing (MeRIP-seq)[6], direct RNA sequencing (DRS)[7], and m^{6}A-sensitive RNA endoribonuclease-facilitated sequencing (m^{6}A-REF-seq)[8]. It was reported that m^{6}A modifications occur in ~30% of transcripts[9]. In addition to mRNAs, it has gradually been accepted that m^{6}A modification occurs in nearly all types of RNAs, such as tRNAs, rRNAs, circRNAs, miRNAs, and lncRNAs[2,10,11]. Most m^{6}A sites are found within the conserved DRACH sequence motif, where D represents G/A/U, R stands for G/A, and H corresponds to A/U/C[9,12–14]. The dynamic regulation of m^{6}A modifications is precisely controlled. This process involves the m^{6}A methyltransferases, known as 'writers', and demethylases, referred to as 'erasers', which play key roles in adding and removing m^{6}A methylation modifications[1,2]. Several writer proteins have been identified, such as METTL3/14/16, RBM15/15B, ZC3H3, VIRMA, CBLL1, WTAP, and KIAA1429[1,2,15–20]. Meanwhile, FTO and ALKBH5 are well-characterized erasers that are responsible for the removal of m^{6}A modifications[1,15].

The biological roles of m^{6}A modifications mostly depend on the recognition of m^{6}A-binding proteins known as m^{6}A readers[21]. These reader proteins recruit various complexes to regulate RNA's metabolism, splicing, translation, stability, translocation, and structures[2,15,22]. To date, a series of reader proteins have been identified and characterized, such as YT521-B homology (YTH) domain-containing proteins, heterogeneous nuclear ribonucleoprotein A2/B1 (hnRNPA2/B1), heterogeneous nuclear ribonucleoproteins C (hnRNP C), heterogeneous nuclear ribonucleoprotein G (hnRNPG), insulin-like growth factor II mRNA-binding protein 1/2/3 (IGF2BP1/2/3), and eukaryotic initiation factor 3 (eIF3)[23,24–28]. Notably, although YTH domain-containing proteins are well-established m^{6}A readers, the roles of other proteins, such as hnRNPA2/B1, IGF2BP1/2/3, hnRNPC, hnRNPG, and eIF3, in m^{6}A recognition remain controversial[23,28]. Hence, YTH domain-containing proteins have been extensively studied across various organisms. The YTH domain, consisting of 100–150 residues, is evolutionarily conserved with the ability to recognize the m^{6}A modifications[29]. Generally, these *YTH domain-containing* genes can be categorized into three subfamilies comprising five distinct members: the YTHDF subfamily (YTHDF1/2/3), the YTHDC1 subfamily (YTHDC1), and the YTHDC2 subfamily (YTHDC2)[11,30,31].

The accumulating documents have revealed that YTH domain-containing genes play diverse roles in the regulation of RNA's stability, splicing, export, and translation. Studies have proven that *YTHDF1* can promote mRNA translation[32,33], *YTHDF2* contributes to the degradation of mRNAs by reducing stability[34,35], and *YTHDF3* was reported to either promote translation or facilitate mRNA degradation[34]. *YTHDC1* is involved in RNA splicing and

nuclear–cytoplasmic transport[36,37], whereas *YTHDC2* is implicated in enhancing the translation efficiency of the target mRNAs[38,39]. For example, in higher vertebrates, *YTH domain-containing* genes have been systematically characterized and extensively investigated for their roles in responding to both abiotic and biotic stresses[40]. The repressed expression of *YTHDF2* or *YTHDF1* markedly enhances the activity of interferon-stimulated genes, creating an antiviral environment that inhibits the replication of both VacV and HSV-1[35]. In mouse (*Mus musculus*), *YTHDF1* deficiency has been shown to limit lysosomal protease expression in dendritic cells (DCs), thereby enhancing cross-presentation and boosting the effectiveness of $CD8^+$ T cell responses against tumor cells[41]. However, despite their crucial roles in recognizing m^6A modifications, reports on *YTH domain-containing* genes in teleosts remain limited, and these have only been reported in zebrafish (*Danio rerio*) and rainbow trout (*Oncorhynchus mykiss*)[40,42]. During the embryonic development of zebrafish, *YTHDF2* promotes the clearance of maternal mRNAs by recognizing m^6A modifications[42]. Furthermore, *YTHDC2* mutants exhibit infertility, highlighting its crucial function in germ cell development in zebrafish[39]. Following heat stress, the expression levels of *OmDF1*, *OmDF2*, *OmDF3*, *OmDC1b*, and *OmDC2* are significantly upregulated, indicating their potential roles in the high-temperature response of rainbow trout[40]. Meanwhile, in rice (*Oryza sativa*), loss-of-function *YTHDFA* mutants exhibited enhanced salinity tolerance, whereas *YTHDFC* mutants showed increased sensitivity to abiotic stresses[43]. In *Camellia chekiangoleosa*, most *CchYTH* genes exhibited a pattern of initially increasing and then decreasing expression levels as the duration of drought stress extended[44]. *YTH11* has also been reported to regulate the stability of m^6A-modified RNA transcripts, thereby facilitating the abiotic stress response in Arabidopsis (*Arabidopsis thaliana*)[35].

Spotted sea bass (*Lateolabrax maculatus*) is natively distributed along the northwestern Pacific coast[45]. It has become a promising aquaculture species in China and is widely farmed in both freshwater ponds and seawater cages[46–48]. Recently, the increasing frequency of diseases outbreaks has significantly affected the survival of spotted sea bass, posing a threat to the maricultural industry's development[45]. Moreover, fluctuations in temperature and salinity can adversely affect the physiological state of spotted sea bass[49,50]. Previous studies have shown that YTH domain-containing genes play crucial roles in responses to abiotic and biotic stresses. Despite their functional importance, *LmYTH* domain-containing genes have not been systematically identified or characterized in spotted sea bass. Thus, this study carried out a genome-wide investigation to characterize the *LmYTH domain-containing* genes in spotted sea bass[40]. Phylogenetic analysis, combined with exon counts and length distribution, YTH domain organization, and motif analysis, revealed the evolutionary conservation of YTH domain-containing genes. Additionally, RNA-seq datasets and real-time quantitative polymerase chain reaction (RT-qPCR) results demonstrated the dynamic expression profiles of *LmYTH domain-containing* genes under bacterial infection, temperature fluctuations, and salinity changes. The present study offers a comprehensive perspective on the *LmYTH* genes, shedding light on their potential functional significance in response to abiotic and biotic stresses.

Materials and methods

Identification of *LmYTH domain-containing* genes

To identify *LmYTH domain-containing* genes, the hidden Markov model (HMM) profile for YTH521-B-like domain (PF04146) was retrieved from the Pfam protein database[51]. This HMM profile served as a query to search for candidate *LmYTH domain-containing* genes from all protein-coding sequences using HMMER v3.3.2 with the default settings[52]. Meanwhile, *YTH domain-containing* genes in model vertebrates (human, mouse, and zebrafish) were downloaded from the NCBI database. BLAST analysis was used to verify the accuracy of the candidate *LmYTH domain-containing* genes[48]. The online ProtParam tool was employed to evaluate the intrinsic physicochemical properties[53]. Subcellular localizations were further predicted via the Cell-PLoc 2.0 online platform[54]. Iso-Seq data sourced from the previous study were used to detect alternative splicing events[55].

Phylogenetic analysis

The phylogenetic tree was constructed on the basis of protein sequences from the *LmYTH* candidates and *YTH domain-containing* genes from representative vertebrates. Multiple sequence alignments were performed using Clustal X (v2.0) with the default settings, which include a gap opening penalty of 10, a gap extension penalty of 0.2, the BLOSUM62 substitution matrix, and the complete alignment mode. The tree was then inferred using the maximum likelihood (ML) method, with robustness evaluated by 1,000 bootstrap replicates. Finally, the phylogenetic tree was visualized using the Interactive Tree of Life (iTOL) platform[56].

Gene characteristics and three-dimensional protein structural analysis

The longest transcripts of *YTH domain-containing* genes from mouse, zebrafish, Japanese medaka, European sea bass, and spotted sea bass were extracted from NCBI Gene Transfer Format (GTF) files to obtain information on the gene structure, including exon number and length. Conserved motifs were identified using MEME v5.5.5[57], with the maximum motif counts set to 10. The YTH domain's locations were determined using NCBI Batch CD-Search[58].

The three-dimensional (3D) protein structure of MmYTH was modeled using the SWISS-MODEL database[59,60]. Meanwhile, the protein sequences of *LmYTH* were analyzed using the diffusion-based method in AlphaFold3 to predict their 3D structures. PyMOL v3.0.3 software was used for the visualization of YTH-GC (m^6A) cytosine and uracil (CU) complexes in MmYTH and LmYTH proteins, further investigating their structural conservation. The binding sites for the interactions between m^6A and aromatic cages were obtained from previously published studies[21,30]. Meanwhile, multiple sequence alignments were performed separately for each subfamily using the online tool ESPript 3.0, with the primary to quaternary protein structure information originating from the 3D structures in the present study[60].

Meta-analysis of RNA-seq data

The RNA-seq datasets were retrieved from the public Sequence Read Archive (SRA) database under the following BioProject accession numbers: PRJNA1093234 (*Nocardia seriolae* infection), PRJNA859992 (skeletal muscle cells under different temperatures), PRJNA841263 (*Aeromonas hydrophila* infection), PRJNA755166 (*Aeromonas veronii* infection), PRJNA557367 (temperature changes), PRJNA515986 (acute hypoxia), and PRJNA611641 (alkalinity stress). The experimental designs were as follows.

N. seriolae infection experiment: Spotted sea bass (average weight 53.22 ± 9.0 g) were randomly assigned to two groups—control and treatment—with each group cultured in three replicate tanks (60 individuals per tank). Following anesthesia, the treatment group was administered an intraperitoneal injection of 100 μL of an *N. seriolae* suspension at a concentration of 1×10^6 colony-forming units (CFU)/mL, while the control group received an equivalent volume of phosphate-buffered saline (PBS). Spleen samples were subsequently collected at 0, 48, 96, and 120 h post-injection, immediately flash-frozen in liquid nitrogen, and stored at –80 °C. Twelve

RNA-seq libraries were prepared, comprising three replicates per group at each time point, and sequenced on the Illumina platform.

A. hydrophila infection experiment: Spotted sea bass (400 ± 50 g) were divided into two groups, one of which was intraperitoneally injected with *A. hydrophila* (1×10^7 CFU/mL), while the control group received an equivalent volume of PBS. Intestinal tissues from both groups were collected at 24 h post-injection, and immediately frozen in liquid nitrogen. Ten sequencing libraries were prepared (five replicates per group) and submitted for sequencing on the Illumina platform.

A. veronii infection experiment: 50 spotted sea bass (8 ± 1 g) were intraperitoneally injected with *A. veronii* at a dose of 8.5×10^5 CFU/g (LD50), while 20 fish received an equivalent volume of 0.85% saline. Spleen tissues were collected at 0, 8, and 24 h post-infection. Nine sequencing libraries were prepared (three replicates per group) and submitted for sequencing on the Illumina platform.

Hypoxia challenge experiment: 60 healthy spotted sea bass (178.25 ± 18.56 g) were transferred into three tanks (20 fish per tank). Oxygen levels were reduced to 1.1 ± 0.14 mg/L within 1 h by adding nitrogen gas, and the hypoxia experiment lasted for 12 h. Oxygen levels were monitored every 10 min. Gill tissues were collected from three fish per tank at 0, 3, 6, and 12 h, then used for RNA extraction. Twelve sequencing libraries were prepared (three replicates per time point) and submitted for sequencing on the Illumina platform.

Alkalinity challenge experiment: Spotted sea bass juveniles were acclimated from seawater to freshwater for 30 days before exposure to alkaline water (carbonate alkalinity: 18 ± 0.2 mmol/L) for 3 days. Gill tissues were sampled at 0, 12, 24, and 72 h post-exposure for RNA extraction. Total RNA from three individuals per tank was pooled into a single sample. Twelve RNA-seq libraries were constructed, with three replicates per group for sequencing on the Illumina platform.

Temperature challenge experiment for tissues: 240 healthy spotted sea bass (2.00 ± 0.01 g) were randomly distributed into eight circular fiberglass tanks (200 L), with 30 fish per tank. These tanks were equally divided into two groups, with water temperatures maintained at either 27 or 33 °C for 8 weeks. At the end of the experiment, nine fish were randomly sampled from each tank and anesthetized. Total RNA was extracted from liver and spleen tissues. Twelve RNA samples (three replicates per treatment) were prepared for transcriptome sequencing.

Temperature challenge experiment for cells: Dorsal white skeletal muscle (approximately 1 cm^3) was excised from anesthetized spotted sea bass (28.46–31.35 g). The tissue was washed, adipose tissue was removed, and the remianing muscle was minced into small pieces before being placed in a cell culture chamber with a growth medium. Cells were cultured at 25 °C in a CO_2-free incubator to support cell migration and passage. When cells reached approximately 70% confluency, they were subcultured using trypsin, and fibroblasts were removed through pre-incubation. The cells were then divided into two groups: A proliferating group, where they were maintained in the growth medium, and a differentiating group, where they were induced to differentiate using a differentiation medium. Each group was further divided into three subgroups and cultured at 21, 25, and 28 °C. Eighteen sequencing libraries were prepared (three replicates per group) and submitted for sequencing on the Illumina platform.

Raw reads were processed with fastp software (using a -q 20 cutoff) to trim and filter, yielding clean reads. Quality assessment of these clean reads was subsequently performed with FastQC software. High-quality reads were then aligned to the reference genome using hisat2 software with the default settings, and the resulting alignments were sorted and saved in BAM format. The count matrix was generated to quantify the number of reads mapped to each *LmYTH* domain-containing gene. The expression levels were normalized and represented as fragments per kilobase of transcripts per million mapped reads (FPKM). Differential expression analysis of the *LmYTH domain-containing* genes was performed using the DESeq2 (v1.44.0), applying stringent criteria of $|\log_2\text{Fold Change}| \geq 1$ and a false discovery rate (FDR) of < 0.05[61,62].

Salinity experiment

A total of 90 healthy spotted sea bass juveniles (body weight 45 ± 5 g) were obtained from the National Aquatic Technology Promotion Station, Beijing Freshwater Breeding Demonstration Base. Prior to the salinity experiment, fish were randomly distributed into six tanks (0.6 m × 0.3 m × 0.4 m; 72 L), with 15 individuals per tank for the two-week acclimation period. Environmental conditions were tightly controlled: Water temperature was held at 15 ± 0.5 °C using a semiautomatic temperature regulation system, dissolved oxygen levels ranged from 6 to 8 mg/L, pH was stabilized between 7.6 and 7.8, salinity was kept at 1‰ ± 0.5‰, and a 12 h light/12 h dark photoperiod was applied. After the acclimation, the tanks were randomly assigned into control and treatment groups. Salinity in the control group was kept at 0‰, while sea salt (Yier Sea Salt, Brand: Fisherman; product number: 10070170378869) mixed with fresh water was used to gradually increase the salinity in the treatment group at a steady rate of 5‰ per day until it reached 30‰. The survival rate of the experimental fish remained at 100% throughout the experiment. After 24 h of adaptation to 30‰ salinity, three fish per tank were randomly selected and anaesthetized with 40 mg/L MS-222 (3-aminobenzoic acid ethyl ester methane-sulfonate). Gill tissues were rapidly collected for RNA extraction.

RNA extraction and RT-qPCR experiment

Total RNA was extracted from the gill tissues in both the control and treatment groups using the traditional Trizol method. RNA from three individuals per tank was pooled to reduce individual variability. High-quality RNA was then used for cDNA synthesis.

Gene-specific primers were designed using Primer 5 software, and the details are provided in Supplementary Table S1. RT-qPCR was performed using the ChamQ SYBR Colour RT-qPCR Master Mix kit (Vazyme, Nanjing, China), following the manufacturer's instructions. Each experimental condition was performed in triplicate at the biological level, with each biological replicate being analyzed in three technical replicates. Relative gene expression was calculated using the $2^{-\Delta\Delta CT}$ method, with *18S* rRNA as the internal control. Statistical comparisons were performed using Student's *t*-test, and the results are presented as the mean ± standard error (SE).

Results

Identification of the *LmYTH domain-containing* genes

Overall, six putative *LmYTH domain-containing* genes were comprehensively identified and designated as *LmDF1a*, *LmDF1b*, *LmDF2*, *LmDF3*, *LmDC1*, and *LmDC2*, on the basis of an analysis using HMMER and BLAST (Table 1, Supplementary Figs S1 and S2). Iso-Seq analysis revealed that all *LmYTH* domain-containing genes in spotted sea bass possessed a single transcript, except for *LmDF3*, which had two different transcripts derived from an alternative 3' splice site (A3SS) event (Supplementary Fig. S3). The lengths of the longest transcripts of the *LmYTH* domain-containing genes ranged from 3,274 (*LmDF1b*) to 18,240 bp (*LmDC2*). These genes are distributed across four chromosomes in an uneven pattern in spotted sea bass. Notably, *LmDC2*, which possessed the longest coding sequence (CDS),

Table 1. Characteristics of *YTH domain-containing* genes in *Lateolabrax maculatus*.

Gene name	Gene_ID	Chromosome position	Gene length (bp)	Exon number	CDS (amino acids)	Molecular weight (kDa)	Theoretical pI	Putative localization
LmDF1a	evm.TU.scaffold_235.11	Chr6 (+): 10,274,451–10,282,610	8,160	6	625	68,102.75	8.81	Cytoplasm
LmDF1b	evm.TU.scaffold_11.218	Chr6 (–): 5,887,283–5,890,556	3,274	4	614	66,271.48	7.85	Cytoplasm, nucleus, extracellular matrix
LmDF2	evm.TU.scaffold_8.5	Chr22 (+): 10,207,118–10,215,610	8,493	6	639	68,286.14	8.86	Cytoplasm
LmDF3	evm.TU.scaffold_7.115	Chr4 (–): 11,565,042–11,572,492	7,451	5	629	69,371.54	9.03	Cytoplasm
LmDC1	evm.TU.scaffold_318.9	Chr16 (+): 119,607–131,643	12,037	15	669	76,962.88	6.49	Nucleus
LmDC2	evm.TU.scaffold_71.73	Chr16 (+): 20,863,917–20,882,156	18,240	30	1,356	152,046.47	7.87	Cell membrane, nucleus

exhibited the highest molecular weight of 152,046.47 kDa, more than twice that of the other *YTH domain-containing* genes. The theoretical isoelectric points (pI) ranged from 6.49 (*LmDC1*) to 9.03 (*LmDF3*). The *LmYTH* domain-containing proteins were primarily distributed in the cytoplasm. Additionally, *LmDF1a*, *LmDF2*, and *LmDF3* were also localized in the nucleus.

Phylogenetic tree of *YTH domain-containing* genes

To explore the evolutionary relationships, a phylogenetic tree was constructed, based on 69 full-length amino acid sequences from spotted sea bass, human, mouse, zebrafish, Japanese fugu (*Takifugu rubripes*), large yellow croaker (*Larimichthys crocea*), turbot (*Scophthalmus maximus*), Japanese medaka (*Oryzias latipes*), European sea bass (*Dicentrarchus labrax*), giant grouper (*Epinephelus lanceolatus*), Barramundi perch (*Lates calcarifer*), Japanese flounder (*Paralichthys olivaceus*), chicken (*Gallus gallus*), and Atlantic salmon (*Salmo salar*). As illustrated in Fig. 1, the phylogenetic tree was clustered into five primary clades, corresponding to *YTHDF1*, *YTHDF2*, *YTHDF3*, *YTHDC1*, and *YTHDC2*. The topology was strongly supported by high bootstrap values. Moreover, these clades were grouped into three major clusters, consistent with the subfamily classifications of *YTHDF*, *YTHDC1*, and YTHDC2 subfamilies. These findings further supported the reliability and accuracy of the *LmYTH domain-containing* genes identification in spotted sea bass. Additionally, these results highlighted the evolutionary divergence among YTH domain-containing gene subfamilies in vertebrates.

Gene structure and conserved motif analysis

Gene structure analysis revealed that all the *LmYTH* genes had exon numbers similar to those of their respective clades (Fig. 2). Notably,

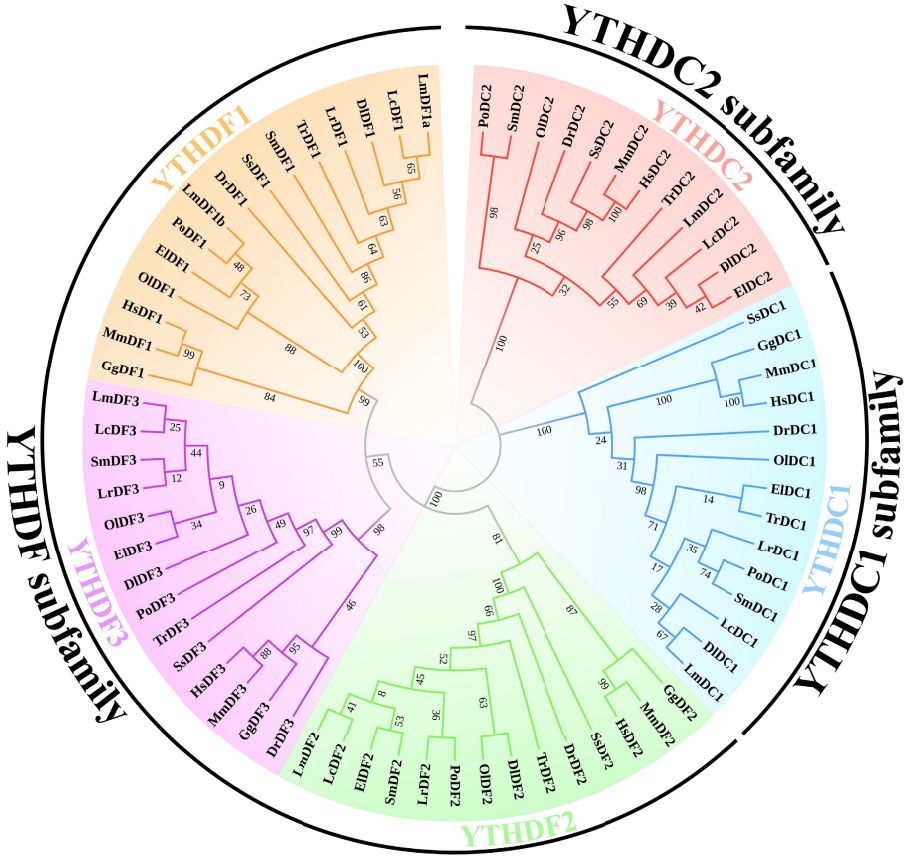

Fig. 1 Phylogenetic tree of *YTH domain-containing* genes. The phylogenetic tree was constructed using the maximum likelihood (ML) method with 1,000 bootstrap replications. Amino acid sequences of the *YTH domain-containing* genes in human, mouse, spotted sea bass, and representative teleosts were aligned to build the phylogenetic tree. The five subclades of *YTHDC1*, *YTHDC2*, *YTHDF1*, *YTHDF2*, and *YTHDF3* are distinguished with different colours. The abbreviations used are as follows: *YTH domain-containing* genes in *Homo sapiens* are labeled as Hs; *Mus musculus*, Mm; *Danio rerio*, Dr; *Dicentrarchus labrax*, Dl; *Epinephelus lanceolatus*, El; *Gallus gallus*, Gg; *Larimichthys crocea*, Lc; *Lateolabrax maculatus*, Lm; *Lates calcarifer*, Lr; *Oryzias latipes*, Ol; *Paralichthys olivaceus*, Po; *Scophthalmus maximus*, Sm; *Salmo salar*, Ss; *Takifugu rubripes*, Tr.

members of the *YTHDC1* and *YTHDC2* subfamilies, particularly the *YTHDC2* subfamily, harbored more exons than those of the *YTHDF* subfamily. The YTH domain, as predicted by the NCBI Batch CD search, was located in the *C*-terminal region of the *YTHDF* and *YTHDC2* subfamilies, whereas the YTH domain of the *YTHDC1* subfamily was positioned in the central region. Members of the *YTHDF* subfamily contained all motifs except Motif 6, suggesting high evolutionary conservation of this subfamily. Motif 6 was found exclusively in the *YTHDC1* and *YTHDC2* subfamilies. Meanwhile, all the members of the *YTHDC1* and *YTHDC2* subfamilies encompassed Motif 1, along with the variable presence of Motifs 3, 4, and 10. The sequence characteristics of the motif sites are shown in Supplementary Fig. S4. In the *YTHDF* subfamily, Motifs 1 and 3 partially overlapped with the YTH domain, although Motif 2 was fully contained in the YTH domain. In the *YTHDC1* and *YTHDC2* subfamilies, Motif 1 partially overlapped with the YTH domain, whereas Motif 6 was entirely contained in the YTH domain.

Interaction analysis between m^{6}A and YTH domain-containing proteins

The 3D protein structure models of YTH domain-containing proteins in mouse and spotted sea bass were constructed and compared to explore the evolutionary conservation in binding ability and pockets to identify m^{6}A modifications (Fig. 3, Supplementary Table S2). YTH domain-containing proteins from mouse and spotted sea bass showed a high degree of structural similarity within the same subfamily, particularly in the YTH domain regions. Notably, the YTH domain exhibited a conserved structural arrangement across all the proteins in both species, characterized by a β-strand at the *N*-terminus and an α-helix at the *C*-terminus. However, the number of α-helices and β-strands in the YTH domains varied slightly among the three subfamilies: the YTHDF subfamily contained 4 α-helices and 8 β-strands, the YTHDC1 subfamily had 4 α-helices and 7 β-strands, and the YTHDC2 subfamily possessed 3 α-helices and 10 β-strands.

In the interactions between RNA molecules and YTH domain-containing proteins, the m^{6}A within the GGACU motif was embedded in an aromatic cage formed by the YTH domain (Fig. 3). The aromatic cage consisted of three hydrophobic amino acid residues (cage residues), which were either tryptophan (W) or leucine (L). The composition of the cage residues was conserved in the homologous YTH domain-containing proteins in mouse and spotted sea bass, but varied among different YTH subfamilies. Specifically, all three cage residues in the YTHDF subfamily were tryptophan, such as W465, W519, and W524 in *LmDF1a*; W465, W519, and W524 in *LmDF1b*; W470, W524, and W529 in *LmDF2*; and W482, W536, and W541 in *LmDF3*. In contrast, the cage residues in the YTHDC1 and YTHDC2 subfamilies were composed of two tryptophan residues and one leucine, such as W337, W388, and L399 in *LmDC1* and W761, W811, and L816 in *LmDC2*. In addition to the aromatic cage, base-specific hydrogen bonds formed with additional hydrophobic amino acid residues, termed hydrogen bond (H-bond) residues, were also essential for the interaction between m^{6}A modifications and YTH domain-containing proteins.

Strong hydrogen bonds (lengths: 2.2–3.0 Å) played important roles in maintaining structural stability. These interactions were visualized in the 3D stick models (Fig. 3). The m^{6}A formed hydrogen bonds with three or four amino acid residues. In both mouse and spotted sea bass, the m^{6}A-modified adenine formed similar hydrogen-bonding interactions with the corresponding amino acid residues.

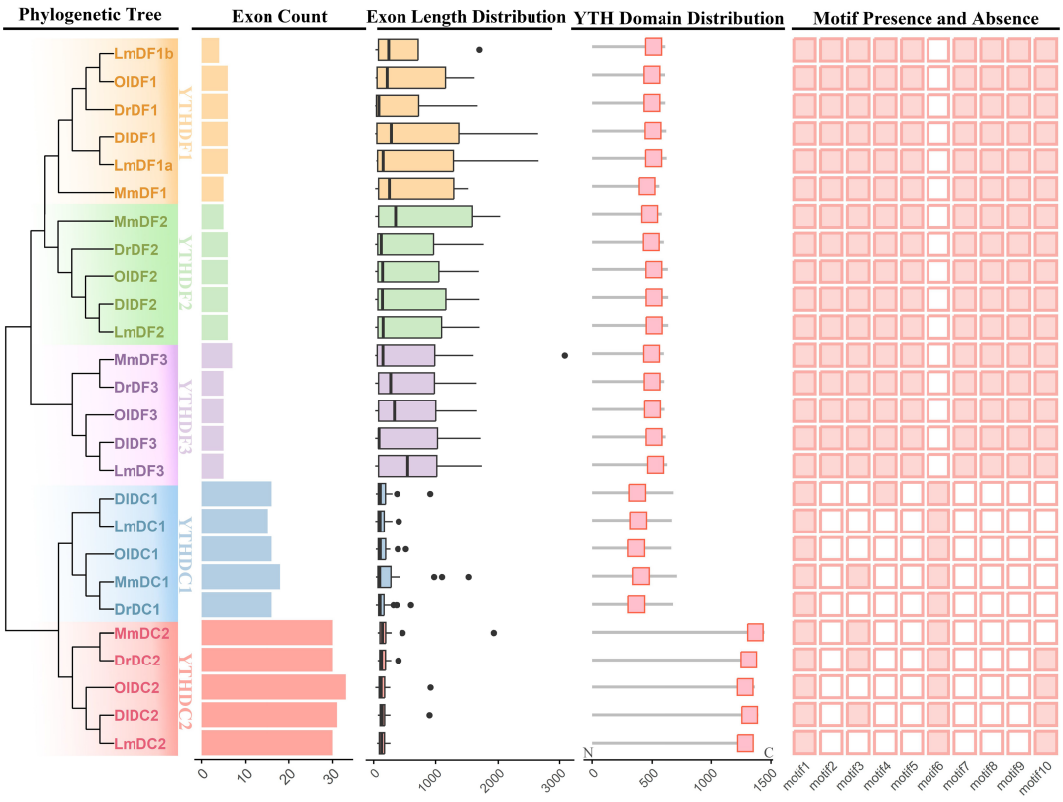

Fig. 2 Gene structure and conserved motif analysis of *YTH domain-containing* genes. Exon counts, exon lengths, the YTH domain's distribution, and conserved motifs were integrated in accordance with the phylogenetic tree that was constructed using the neighbour-joining method with 1,000 bootstrap replications. The five subclades, *YTHDC1*, *YTHDC2*, *YTHDF1*, *YTHDF2*, and *YTHDF3*, are distinguished by distinct colours. The presence and absence of different motifs are represented as solid and open boxes, respectively. The abbreviations used are as follows: *YTH domain-containing* genes in *Mus musculus* are denoted as Mm; *Lateolabrax maculatus*, Lm; *Danio rerio*, Dr; *Oryzias latipes*, Ol; *Dicentrarchus labrax*, Dl.

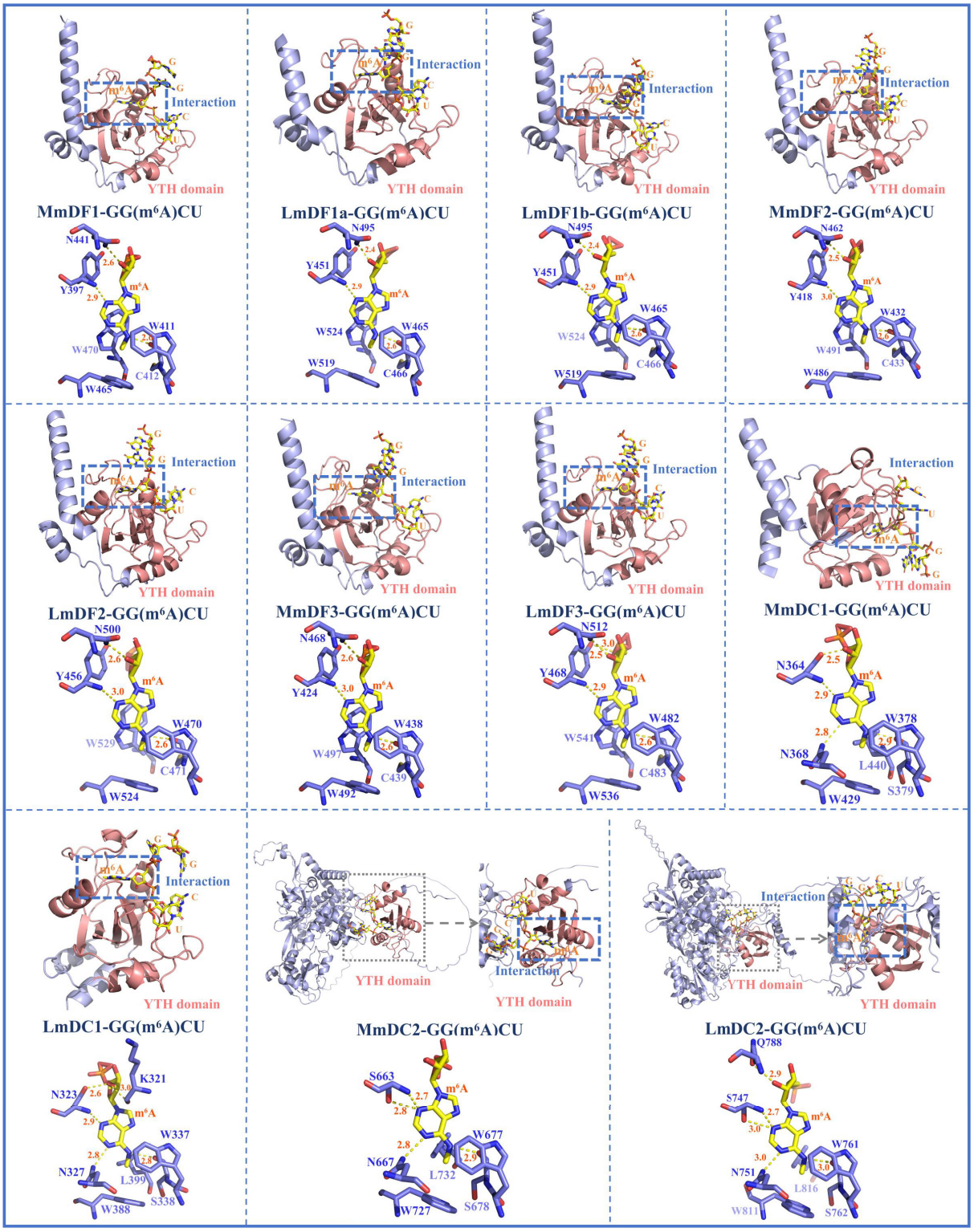

Fig. 3 Three-dimensional protein structure models of *YTH domain-containing* genes and their interactions with m^{6}A-modified adenine. The structure of the YTH domain is depicted in shades of pink. The other secondary structural elements, including α-helices, β-strands, and coils, are marked with cyan colour. In the YTH-GC (m^{6}A) CU complexes, the RNA molecules and m^{6}A modifications are represented with yellow colour, and the amino acid residues of YTH domain-containing proteins are shown with blue colour. Hydrogen bonds between the binding pocket and the m^{6}A modification are indicated using dashed yellow lines (2.2 Å ≤ cutoff ≤ 3.0 Å). Abbreviations: *Mus musculus*, Mm; *Lateolabrax maculatus*, Lm.

Multiple sequence alignment analysis

Multiple sequence alignments were performed to investigate the structural features of the YTH domain in mouse and spotted sea bass (Fig. 4). Compared with the YTHDC2 subfamily, the YTH domain sequences of proteins in the remaining subfamilies were much more conserved between mouse and spotted sea bass, with an identify value of > 82.8%. In contrast, a series of amino acid residues were divergent in the YTHDC2 subfamily of mouse and spotted sea bass

with a relatively low identify value of 71.1%. The three or four amino acids forming strong hydrogen bonds (marked with red points in Fig. 4) were located upstream of the second cage residue, except for L403 in *LmDC1*. Notably, one of them was always adjacent to the first cage residue. Additionally, the amino acids were highly conserved in the neighboring regions of the cage residues and hydrogen bond residues.

Expression patterns of *LmYTH domain-containing* genes in response to biotic and abiotic stresses

Several bacterial species, including *N. seriolae*, *A. hydrophila*, and *A. veronii*, have been reported to pose a serious threat to the health of spotted sea bass. The present study revealed that the expression patterns of several *LmYTH domain-containing* genes were changed after bacterial infection, suggesting their potential roles in the immune response in spotted sea bass (Fig. 5). After *N. seriolae* infection, the expression of *LmDC1* in the spleens was significantly downregulated at 96 h, whereas *LmDF3* was significantly upregulated at 120 h. Although no statistically significant differences were observed, the expression patterns of *LmDF1a*, *LmDF2*, and *LmDF3* showed a similar trend in response to *N. seriolae* infection. In contrast, the expression levels of *LmDF1b*, *LmDC1*, and *LmDC2* remained unchanged after infection. The expression of all the *LmYTH domain-containing* genes was insensitive

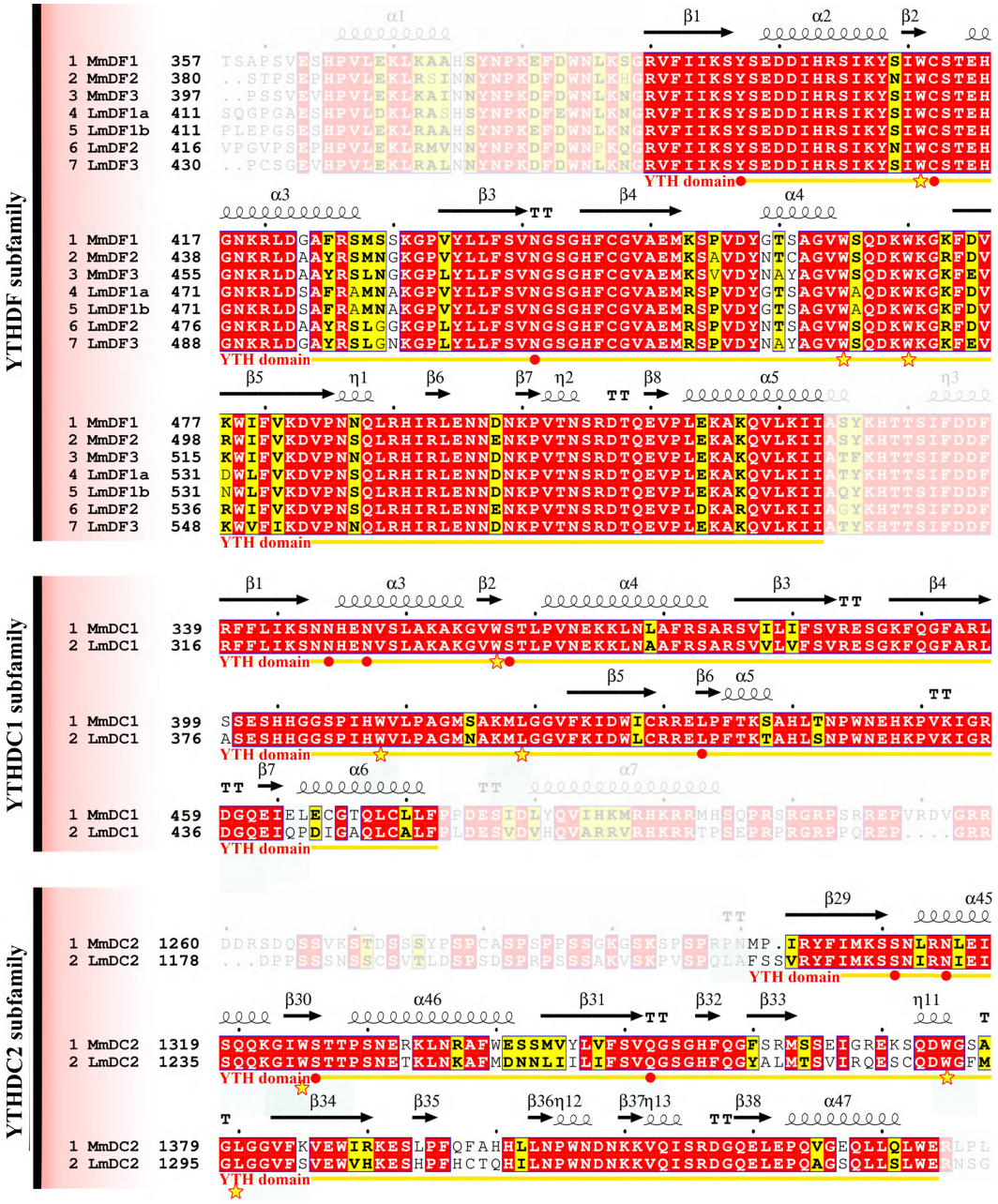

Fig. 4 Multiple sequence alignments of YTH domains in mouse and spotted sea bass. Gene names and the corresponding amino acid positions are presented on the left of the sequence alignments. *YTH domain-containing* genes in mouse and spotted sea bass are designated as Mm and Lm, respectively. Predicted secondary structural elements are displayed above the sequence alignment, with medium squiggles representing α-helices, arrows indicating β-strands, and the letters TT denoting strict β-turns. In the sequence alignment, strictly conserved amino acid residues with 100% identity are highlighted in red with white lettering, whereas highly similar sequences are enclosed in blue frames and marked with blocks. The YTH domain is denoted by yellow arrows below the alignment, the cage residues are denoted by stars, and red solid points represent amino acids with the ability to form hydrogen bonds (hydrogen bond residues).

to the *A. hydrophila* infection in the intestinal tissue of spotted sea bass, although *LmDC1* was abundantly expressed. Meanwhile, *LmDC2* exhibited significant upregulation in the spleens at 8 h after *A. veronii* infection.

LmDF1a, *LmDF2*, *LmDF3*, and *LmDC1* were abundantly expressed in the gill tissues of spotted sea bass, compared with *LmDF1b* and *LmDC2*. No significant changes in the expression of any *LmYTH domain-containing* genes were observed in gill tissues under hypoxia and alkalinity stresses. This suggested that *LmYTH* domain-containing proteins may not act as readers for RNA m^{6}A modification in response to hypoxia and adaptation to alkalinity. Additionally, the expression patterns of all the *LmYTH domain-containing* genes were investigated in liver, spleen, and skeletal muscle cells under different environment temperatures. It was evident that *LmDF1b* showed weak expression, especially in liver tissues. The expression levels of *LmDF1b* and *LmDC1* in skeletal muscle cells cultured at 25 °C were significantly upregulated compared with cells cultured at 21 °C. Notably, *LmDF1a* displayed the opposite expression pattern in skeletal muscle cells compared with the duplicated copies of *LmDF1b*. There appears to be a functional divergence between *LmDF1a* and *LmDF1b* in response to temperature stress.

RT-qPCR analysis of *LmYTH domain-containing* genes under different salinity conditions

To investigate the potential roles of *LmYTH domain-containing* genes in response to different levels of salinity in the environment, RT-qPCR was conducted to evaluate their expression profiles in the gills following exposure to freshwater (0‰) and seawater (30‰). The results revealed that the expression levels of three *LmYTH* domain-containing genes were significantly affected by salinity changes (Fig. 6). In the seawater group, *LmDF1a* was significantly downregulated. In contrast, both *LmDF1b* and *LmDC1* were significantly upregulated in seawater. Interestingly, *LmDF1a* and *LmDF1b*, the duplicated copies, exhibited opposite expression patterns in response to changes in salinity.

Discussion

At present, over 150 distinct RNA modifications with diverse biological functions have been identified in organisms[63]. These RNA modifications introduce additional layers of complexity to post-transcriptional regulation. Among them, m^{6}A is generally accepted as one of the most abundant modifications in eukaryotic transcriptomes across nearly all RNA types, such as mRNAs, rRNAs, tRNAs, and snRNAs[1,2]. Reader

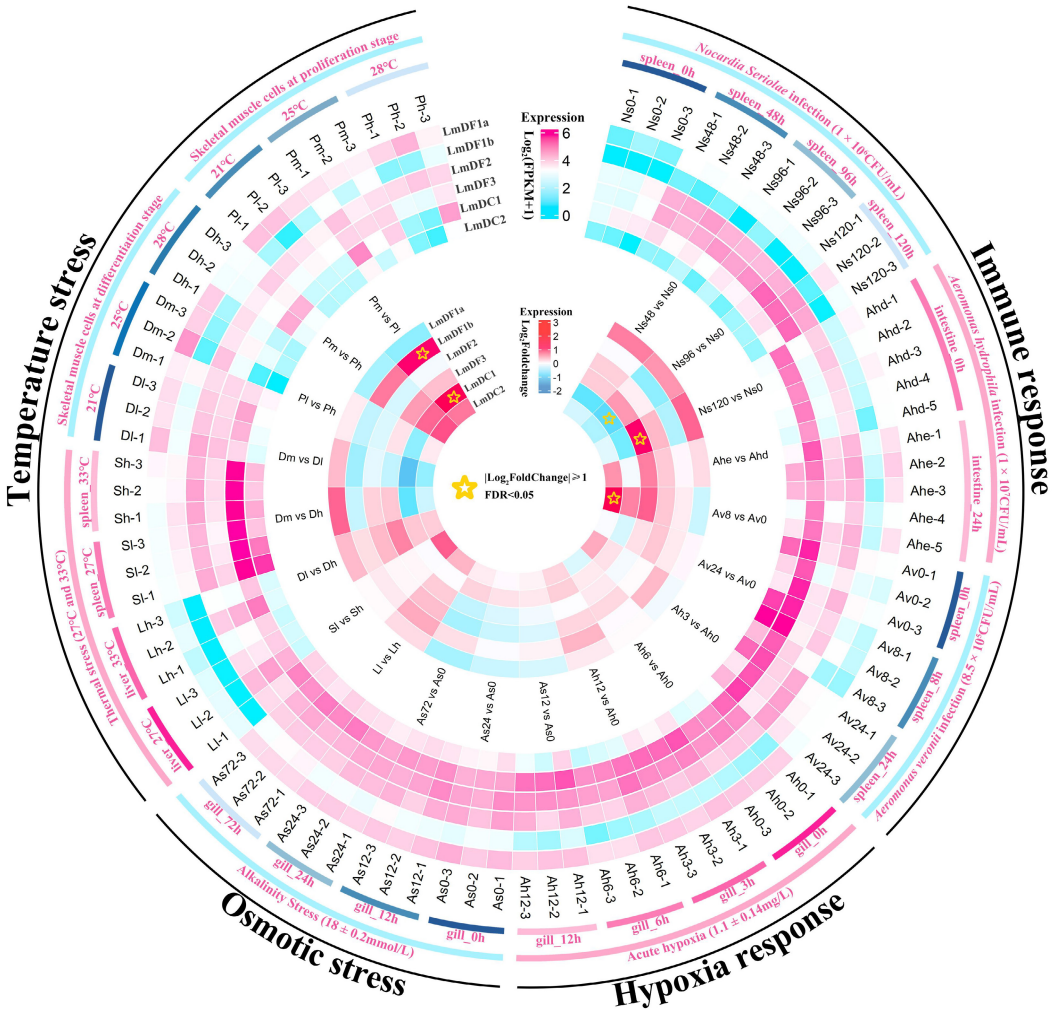

Fig. 5 Expression patterns of *YTH domain-containing* genes in spotted sea bass in response to biotic and abiotic stresses. The expression levels are normalized as the FPKM values and shown as $\log_{10}$(FPKM + 1), which are displayed in the outer heatmap. The significance of differential gene expression was determined using the DESeq2 v1.44.0 R package based on the criteria of | $\log_2$(Fold Change) | ≥ 1 and FDR < 0.05. The differentially expressed genes are marked using stars in the inner heatmap.

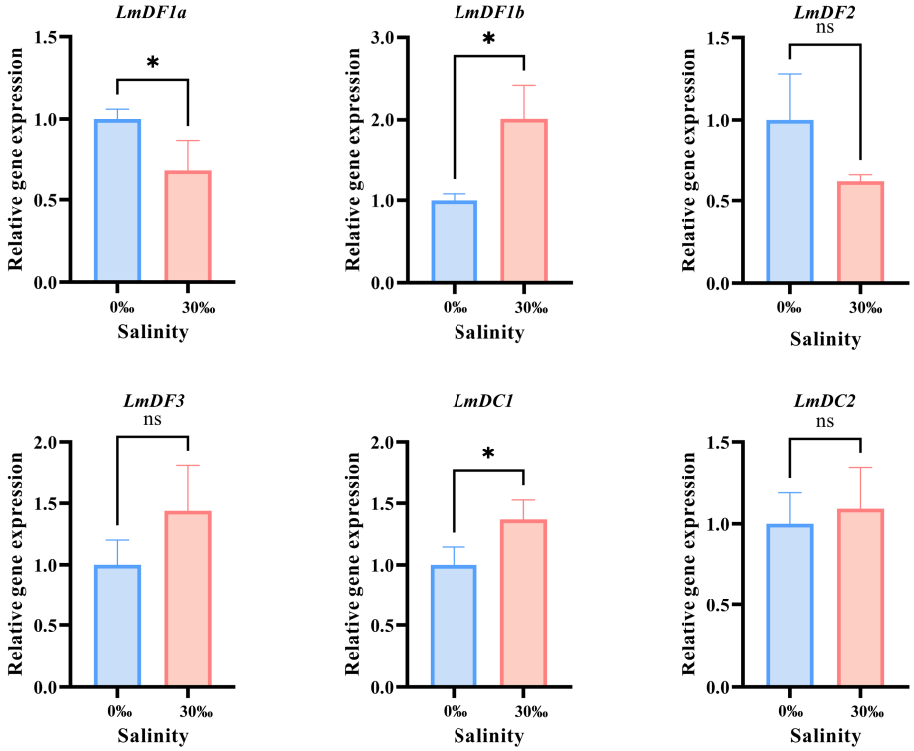

Fig. 6 RT-qPCR verification and statistical analysis. All the RT-qPCR experiments were performed with three biologically independent replicates. The relative expression levels were calculated using the $2^{-\Delta\Delta CT}$ method and normalized against 18S rRNA. Results are presented as the mean ± standard deviation (SD). Asterisks indicate the statistically significant differences (* $p < 0.05$), while 'ns' indicates no significant difference.

proteins are necessary for the functional achievement of m^{6}A modifications. In the last decade, the YTH domain-containing proteins have been widely investigated as acting as readers for the m^{6}A modifications in both plants and animals[29,36]. In the present study, six *LmYTH domain-containing* genes were comprehensively identified and systematically analyzed. Conserved domain features, gene structures, and expression patterns under various stress conditions suggest that these genes may play important roles in response to abiotic and biotic stresses.

The six *LmYTH domain-containing* genes in spotted sea bass can be divided into three subfamilies. Previous studies have identified duplicated or triplicated copies of *YTH domain-containing* genes in rainbow trout, including *OmDF1a*, *OmDF1b*, and *OmDF1c*; *OmDF2a* and *OmDF2b*; and *OmDC1a* and *OmDC1b*[40]. However, only duplicated *YTHDF1* genes were found in spotted sea bass, including *LmDF1a* and *LmDF1b*. The duplication of *YTH domain-containing* genes, originating from the 4R whole-genome duplication specific to salmon, was absent in spotted sea bass[40]. A series of differences in exon count, exon length, YTH domain position, and motif distribution were observed among the YTHDF, YTHDC1, and YTHDC2 subfamilies. The diversity of gene structure highlighted the evolutionary specialization and functional divergence among different YTH subfamilies. The YTH domain was predominantly located in the *C*-terminal region in both the YTHDF and YTHDC2 subfamilies, whereas it was positioned in the central region in the *YTHDC1* subfamily. Similar findings were previously reported in rainbow trout[40]. In contrast, some members of the YTHDF subfamily in the plant alfalfa (*Medicago sativa*) exhibited *N*-terminal distribution of the YTH domain[64]. Motif distribution patterns were conserved within each subfamily. Motif 1 was present in all the YTH domain-containing genes of both spotted sea bass and other vertebrates, such as mouse, zebrafish, medaka, and European sea bass. However, Motif 6 only appeared in the YTHDC1 and YTHDC2 subfamilies. The distribution of the YTH domain and the motifs' presence/absence may be linked to protein structure, enabling efficient interaction with GG (m^{6}A) CU complexes.

Certain motifs were found to overlap with the YTH domain. Previous studies revealed that three shared motifs were identified in all 10 *OmYTH* genes in rainbow trout, all of which overlapped with the YTH domain. Only one motif was present across all members of *LmYTH* genes. Moreover, Motifs 1–3 overlapped with YTH domain in the members of the LmDF subfamily, while Motif 1 and Motif 6 were present in the YTH domain regions of the LmDC1 and LmDC2 subfamilies. These differences may be associated with variations in gene copy numbers in rainbow trout and spotted sea bass. The similarity in motif sequence characteristics suggests the strong evolutionary conservation of YTH domain functions.

The aromatic cage interacted with the m^{6}A residue via a positively charged region formed by the side chains of three specific amino acids[65]. In human and mouse, a WWW-type aromatic cage composed of three tryptophan residues is specific in the structures of proteins encoded by members of the YTHDF subfamily, whereas the YTHDC1 and YTHDC2 proteins have a WWL-type cage consisting of two tryptophan residues and one leucine residue[30,39]. Similar findings were observed in the present study, suggesting a conserved mechanism for m^{6}A recognition. A similar aromatic cage in YTHDF proteins was reported in wheat (*Triticum aestivum* L.), although its YTHDC protein featured a WWY-type cage, in which the leucine (L) was replaced by tyrosine (Y)[15,66]. These observations suggest that the m^{6}A-binding mechanism of YTHDCs differs between plants and animals, further highlighting significant evolutionary divergence in YTH domain-mediated m^{6}A recognition in organisms. In addition, the 3D structures of YTH domain-containing proteins showed considerable similarities, including conserved

patterns of α-helices and β-strands, and similar amino acid residues involved in hydrogen bonding with m^{6}A-modified RNA. These findings indicated a highly analogous structural relationship between mouse and spotted sea bass, offering further support for the evolutionary conservation of YTH domain-containing proteins and their mode of binding to m^{6}A modifications.

The expression patterns of multiple *LmYTH domain-containing* genes, particularly *LmDF1b*, *LmDF3*, *LmDC1*, and *LmDC2*, were altered in response to abiotic and biotic stresses. These findings suggested that *LmYTH domain-containing* genes might play important roles in stress response, similar to those observed in zebrafish and miiuy croaker (*Miichthys miiuy*)[42,67]. Previous studies have confirmed that *YTHDF3* can regulate the decay of methylated mRNA and promote protein synthesis, thereby exacerbating inflammation in response to bacterial infection[5,34]. Meanwhile, *YTHDC1* and *YTHDC2* could regulate the expression of immunity-related genes[68,69]. For instance, *YTHDC1* was significantly upregulated in patients with Type 1 diabetes mellitus (T1DM), showing a strong correlation with differentially expressed transcripts[70]. In teleosts, the spleen is one of the most important immune organs, playing a key role in response to bacterial infections. These reports are consistent with our findings that *LmDF3* was significantly upregulated in the spleen after 120 h after *N. seriolae* infection, and *LmDC2* showed elevated expression following *A. veronii* infection. In contrast, the expression of *LmDC1* was significantly downregulated at 96 h after *N. seriolae* infection, indicating that the host might have suppressed translation efficiency and accelerated mRNA degradation in the spleen as part of the immune response to bacterial challenge. In mouse, co-transcriptionally deposited m^{6}A has been shown to be crucial for the heat stress response[60]. Heat stress was found to reshape the genomic distribution of *YTHDC1* in humans, which binds to m^{6}A-modified heat-induced heat shock protein (HSP) RNAs, promoting HSP expression[37]. It was also reported that in humans, the expression of *YTHDF2* significantly increased after heat stress, while *YTHDF1* exhibited a more moderate increase[71]. The current study also yielded similar results, with *LmDF1b* and *LmDC1* being significantly upregulated in proliferating skeletal muscle cells at 25 °C compared with those at 21 °C. In contrast, *LmDF1a* and *LmDF2* exhibited a decreasing trend in expression. The significant upregulation of *LmDF1b* and *LmDC1* might have been linked to cell proliferation, as elevated temperatures were found to promote the proliferation of skeletal muscle cells, a process characterized by highly active transcription and translation. In humans, *YTHDF1* and *YTHDC2* were shown to promote cell proliferation, which could further explain the significant upregulation of *LmYTH domain-containing* genes[41]. This expression pattern suggested that *LmYTH domain-containing* genes may contribute to transcriptionally active states associated with cell proliferation, consistent with their known roles in modulating gene expression dynamics in proliferating cells.

As a typical euryhaline teleost, spotted sea bass can live in both freshwater and seawater, exhibiting strong salinity tolerance and osmoregulatory capabilities. RT-qPCR analysis revealed distinct expression patterns of *LmYTH domain-containing* genes under freshwater and seawater conditions. For instance, *LmDF1b* and *LmDC1* were significantly upregulated, whereas *LmDF1a* was downregulated. In alfalfa, *MsYTH2* was predominantly expressed under salinity conditions, and stress-related *cis*-elements were identified in the upstream regions of YTH members' promoters, suggesting their responsiveness to environmental stressors[64]. Additionally, motifs enriched in specific amino acids, such as the leucine-rich repeat domain, were associated with salt resistance[64]. However, the leucine-rich repeat domain was absent in the proteins encoded by *LmYTH domain-containing* genes. Although RT-qPCR validation under salinity stress alone cannot conclusively demonstrate the functional roles of these genes, the observed expression differences, especially the opposite regulation of the duplicated genes *LmDF1a* and *LmDF1b*, suggest their potential functional divergence in response to salinity adaptation. Nevertheless, additional experiments are required to further validate the specific functions.

Conclusions

The present study systematically identified and characterized six members of *LmYTH domain-containing* genes, which can be divided into the YTHDF, YTHDC1, and YTHDC2 subfamilies. Similar gene structures, YTH domain distributions, and motif sites were observed between mouse and spotted sea bass. In addition, proteins encoded by *LmYTH* genes shared similar α-helices and β-strand compositions in their 3D structures, the same WWW- or WWL-type aromatic cages for m^{6}A recognition, and common amino acid residues for hydrogen bond formation in mouse and spotted sea bass. These findings suggested the evolutionary conservation of m^{6}A binding ability in YTH domain-containing genes. Upon bacterial infection, *LmDF3* and *LmDC2* were observed to be significantly upregulated, whereas *LmDC1* was significantly downregulated. Meanwhile, *LmDF1b* and *LmDC1* were significantly upregulated in the skeletal muscle cells at the proliferation stage after exposure to different temperatures. Under different salinity conditions, *LmDF1a* was significantly downregulated, whereas *LmDF1b* and *LmDC1* were significantly upregulated. These results indicated their important roles in responding to abiotic and biotic stresses. In addition, it was interesting that *LmDF1a* and *LmDF1b*, the duplicated copies, displayed opposite expression trends when treated with the same temperatures or salinity conditions. This study systematically characterized six *LmYTH domain-containing* genes, highlighting their conserved structures that enable interactions with m^{6}A-modified RNA. Additionally, the findings suggest the potential functional divergence of *LmDF1*, requiring further investigations.

Ethical statements

All animal experiments were approved by the Animal Research and Ethics Committees of Ocean University of China (Permit No. 20141201) and conducted in accordance with the relevant ethical guidelines. No endangered or protected species were involved in this study.

Author contributions

The authors confirm contribution to the paper as follows: conceptualization: Zhu H, Tian Y; formal analysis: Zhu H; investigation: Zhu H, Qi X; resources: Zhu H, Yan C; software: Zhu H, Zhang J, Wang B; visualization: Zhu H; data curation: Zhu H, Yu H, Tian Y; writing – original draft preparation: Zhu H; writing – reviewing and editing: Gao Q, Tian Y; methodology: Li Y, Wen H, Gao Q, Tian Y; supervision: Li Y, Wen H, Gao Q, Tian Y; validation: Qi X, Lu Y, Yao Y; project administration: Gao Q, Tian Y; funding acquisition: Gao Q, Tian Y. All authors reviewed the results and approved the final version of the manuscript.

Data availability

The transcriptome datasets analyzed in the current study were obtained from the NCBI database: PRJNA1093234 (*Nocardia seriolae* infection), PRJNA859992 (skeletal muscle cells under different temperatures), PRJNA841263 (*Aeromonas hydrophila*), PRJNA755166 (*Aeromonas veronii*), PRJNA557367 (temperature changes), PRJNA515986 (acute hypoxia) and PRJNA611641 (alkalinity stress).

Acknowledgments

This study was supported by the Shandong Provincial Natural Science Foundation (ZR2022QC086), the China National Postdoctoral Program for Innovative Talents (BX20240343), the National Natural Science Foundation of China (32202896), the National Natural Science Foundation of China (32373104), the Key R&D Project of Shandong Province (2022ZLGX01), the China Postdoctoral Science Foundation (2022M713001), the Marine Science and Technology Innovation Demonstration Project of Qingdao (23-1-3-hysf-2-hy), the Key Research and Development Program of Shandong Province (2021SFGC0701), and the Technology Plan Project of Tangshan (23130233E).

Conflict of interest

The authors declare that they have no conflict of interest.

Supplementary information accompanies this paper at (https://www.maxapress.com/article/doi/10.48130/gcomm-0025-0020)

Dates

Received 21 May 2025; Revised 22 July 2025; Accepted 1 September 2025; Published online 24 October 2025

References

1. He PC, He C. 2021. m^{6}A RNA methylation: from mechanisms to therapeutic potential. *The EMBO Journal* 40:e105977
2. Jiang X, Liu B, Nie Z, Duan L, Xiong Q, et al. 2021. The role of m^{6}A modification in the biological functions and diseases. *Signal Transduction and Targeted Therapy* 6(1):74
3. Dunn DB, Smith JD. 1955. Occurrence of a new base in the deoxyribonucleic acid of a strain of bacterium coli. *Nature* 175:336–37
4. Desrosiers R, Friderici K, Rottman F. 1974. Identification of methylated nucleosides in messenger RNA from novikoff hepatoma cells. *Proceedings of the National Academy of Sciences of the United States of America* 71(10):3971–75
5. Perry RP, Kelley DE. 1974. Existence of methylated messenger RNA in mouse L cells. *Cell* 1(1):37–42
6. Chen J, Zhang YC, Huang C, Shen H, Sun B, et al. 2019. m^{6}A regulates neurogenesis and neuronal development by modulating histone methyltransferase Ezh2. *Genomics, Proteomics & Bioinformatics* 17(2):154–68
7. Workman RE, Tang AD, Tang PS, Jain M, Tyson JR, et al. 2019. Nanopore native RNA sequencing of a human poly(A) transcriptome. *Nature Methods* 16:1297–305
8. Zhang Z, Chen LQ, Zhao YL, Yang CG, Roundtree IA, et al. 2019. Single-base mapping of m^{6}A by an antibody-independent method. *Science Advances* 5(7):eaax0250
9. Dominissini D, Moshitch-Moshkovitz S, Schwartz S, Salmon-Divon M, Ungar L, et al. 2012. Topology of the human and mouse m^{6}A RNA methylomes revealed by m^{6}A-seq. *Nature* 485:201–6
10. Liu Y, Yang D, Liu T, Chen J, Yu J, et al. 2023. N^6-methyladenosine-mediated gene regulation and therapeutic implications. *Trends in Molecular Medicine* 29(6):454–67
11. Shi H, Wei J, He C. 2019. Where, when, and how: context-dependent functions of RNA methylation writers, readers, and erasers. *Molecular Cell* 74(4):640–50
12. Chen K, Luo G-Z, He C. 2015. Chapter nine-high-resolution mapping of *N*^{6}-methyladenosine in transcriptome and genome using a photo-crosslinking-assisted strategy. *Methods in Enzymology* 560:161–85
13. Fu Y, Dominissini D, Rechavi G, He C. 2014. Gene expression regulation mediated through reversible m^{6}A RNA methylation. *Nature Reviews Genetics* 15:293–306
14. Jiang C, Li P, Ma Y, Yoneda N, Kawai K, et al. 2024. Comprehensive gene profiling of the metabolic landscape of humanized livers in mice. *Journal of Hepatology* 80:622–33
15. Yang Y, Hsu PJ, Chen YS, Yang YG. 2018. Dynamic transcriptomic m^{6}A decoration: writers, erasers, readers and functions in RNA metabolism. *Cell Research* 28:616–24
16. Patil DP, Chen CK, Pickering BF, Chow A, Jackson C, et al. 2016. m^{6}A RNA methylation promotes XIST-mediated transcriptional repression. *Nature* 537:369–73
17. Bokar JA, Shambaugh ME, Polayes D, Matera AG, Rottman FM. 1997. Purification and cDNA cloning of the AdoMet-binding subunit of the human mRNA (*N*^{6}-adenosine)-methyltransferase. *RNA* 3(11):1233–47
18. Liu J, Yue Y, Han D, Wang X, Fu Y, et al. 2014. A METTL3–METTL14 complex mediates mammalian nuclear RNA *N*^{6}-adenosine methylation. *Nature Chemical Biology* 10:93–95
19. Schwartz S, Mumbach MR, Jovanovic M, Wang T, Maciag K, et al. 2014. Perturbation of m6A writers reveals two distinct classes of mRNA methylation at internal and 5′ sites. *Cell Reports* 8(1):284–96
20. Liu C, Fan D, Sun J, Li G, Du R, et al. 2025. Inhibition of METTL14 overcomes CDK4/6 inhibitor resistance driven by METTL14-m^{6}A-E2F1-axis in ERα-positive breast cancer. *Journal of Nanobiotechnology* 23:3
21. Patil DP, Pickering BF, Jaffrey SR. 2018. Reading m^{6}A in the transcriptome: m^{6}A-binding proteins. *Trends in Cell Biology* 28:113–27
22. Shi H, Chai P, Jia R, Fan X. 2020. Novel insight into the regulatory roles of diverse RNA modifications: re-defining the bridge between transcription and translation. *Molecular Cancer* 19:78
23. Mo L, Meng L, Huang Z, Yi L, Yang N, et al. 2022. An analysis of the role of HnRNP C dysregulation in cancers. *Biomarker Research* 10:19
24. Meyer KD, Patil DP, Zhou J, Zinoviev A, Skabkin MA, et al. 2015. 5' UTR m^{6}A promotes cap-independent translation. *Cell* 163(4):999–1010
25. Wang X, Lu Z, Gomez A, Hon GC, Yue Y, et al. 2014. *N*^{6}-methyladenosine-dependent regulation of messenger RNA stability. *Nature* 505:117–20
26. Huang H, Weng H, Sun W, Qin X, Shi H, et al. 2018. Recognition of RNA *N*^{6}-methyladenosine by IGF2BP proteins enhances mRNA stability and translation. *Nature Cell Biology* 20:285–95
27. Yang J, Yang Q, Huang X, Yan Z, Wang P, et al. 2023. METTL3-mediated LncRNA *EN_42575* m6A modification alleviates CPB2 toxin-induced damage in IPEC-J2 cells. *International Journal of Molecular Sciences* 24(6):5725
28. Zhou KI, Shi H, Lyu R, Wylder AC, Matuszek Ż, et al. 2019. Regulation of co-transcriptional pre-mRNA splicing by m^{6}A through the low-complexity protein hnRNPG. *Molecular Cell* 76:70–81.e9
29. Stoilov P, Rafalska I, Stamm S. 2002. YTH: a new domain in nuclear proteins. *Trends in Biochemical Sciences* 27(10):495–97
30. Liao S, Sun H, Xu C. 2018. YTH domain: a family of *N*^{6}-methyladenosine (m^{6}a) readers. *Genomics, Proteomics & Bioinformatics* 16(2):99–107
31. Zhang Z, Theler D, Kaminska KH, Hiller M, de la Grange P, et al. 2010. The YTH domain is a novel RNA binding domain. *Journal of Biological Chemistry* 285(19):14701–10
32. Wang X, Zhao BS, Roundtree IA, Lu Z, Han D, et al. 2015. *N*^{6}-methyladenosine modulates messenger RNA translation efficiency. *Cell* 161(6):1388–99
33. Ma W, Cui S, Lu Z, Yan X, Cai L, et al. 2022. YTH domain proteins play an essential role in rice growth and stress response. *Plants* 11(17):2206
34. Cheng X, Yao S, Zhang J, Wang D, Xu S, et al. 2024. Genome-wide identification and expression analysis of YTH gene family for abiotic stress regulation in camellia chekiangoleosa. *International Journal of Molecular Sciences* 25(7):3996
35. Amara U, Hu J, Park SJ, Kang H. 2024. ECT12, an YTH-domain protein, is a potential mRNA m^{6}A reader that affects abiotic stress responses by modulating mRNA stability in *Arabidopsis*. *Plant Physiology and Biochemistry* 206:108255
36. Zong X, Xiao X, Shen B, Jiang Q, Wang H, et al. 2021. The *N*^{6}-methyladenosine RNA-binding protein YTHDF1 modulates the translation of *TRAF6* to mediate the intestinal immune response. *Nucleic Acids Research* 49(10):5537–52
37. Shi H, Wang X, Lu Z, Zhao BS, Ma H, et al. 2017. YTHDF3 facilitates translation and decay of *N*^{6}-methyladenosine-modified RNA. *Cell Research* 27:315–28

38. Hesser CR, Walsh D. 2023. YTHDF2 is downregulated in response to host shutoff induced by DNA virus infection and regulates interferon-stimulated gene expression. *Journal of Virology* 97:e01758-22
39. Xiao W, Adhikari S, Dahal U, Chen YS, Hao YJ, et al. 2016. Nuclear m^{6}A reader YTHDC1 regulates mRNA splicing. *Molecular Cell* 61(4):507–19
40. Timcheva K, Dufour S, Touat-Todeschini L, Burnard C, Carpentier MC, et al. 2022. Chromatin-associated YTHDC1 coordinates heat-induced reprogramming of gene expression. *Cell Reports* 41:111784
41. Hsu PJ, Zhu Y, Ma H, Guo Y, Shi X, et al. 2017. Ythdc2 is an *N*^{6}-methyladenosine binding protein that regulates mammalian spermatogenesis. *Cell Research* 27:1115–27
42. Li L, Krasnykov K, Homolka D, Gos P, Mendel M, et al. 2022. The XRN1-regulated RNA helicase activity of YTHDC2 ensures mouse fertility independently of m^{6}A recognition. *Molecular Cell* 82(9):1678–1690.e12
43. Yu H, Gao Q, Wang W, Liu D, He J, et al. 2023. Comprehensive analysis of YTH domain-containing genes, encoding m^{6}A reader and their response to temperature stresses and *Yersinia ruckeri* infection in rainbow trout (*Oncorhynchus mykiss*). *International Journal of Molecular Sciences* 24(11):9348
44. Li F, Zeng C, Liu J, Wang L, Yuan X, et al. 2024. The YTH domain-containing protein family: Emerging players in immunomodulation and tumour immunotherapy targets. *Clinical and Translational Medicine* 14(8):e1784
45. Shao C, Li C, Wang N, Qin Y, Xu W, et al. 2018. Chromosome-level genome assembly of the spotted sea bass, *Lateolabrax maculatus*. *GigaScience* 7(11):giy114
46. Zhang X, Wen H, Wang H, Ren Y, Zhao J, et al. 2017. RNA-Seq analysis of salinity stress–responsive transcriptome in the liver of spotted sea bass (*Lateolabrax maculatus*). *PLoS One* 12(3):e0173238
47. Zhu Q, Li M, Lu W, Wang Y, Li X, et al. 2023. Transcriptomic modulation reveals the specific cellular response in Chinese Sea Bass (*Lateolabrax maculatus*) gills under salinity change and alkalinity stress. *International Journal of Molecular Sciences* 24(6):5877
48. Chen C, Wu Y, Li J, Wang X, Zeng Z, et al. 2023. TBtools-II: A 'one for all, all for one' bioinformatics platform for biological big-data mining. *Molecular Plant* 16(11):1733–42
49. Guo J, Wang L, Song K, Lu K, Li X, et al. 2023. Physiological response of spotted seabass (*Lateolabrax maculatus*) to different dietary available phosphorus levels and water temperature: changes in growth, lipid metabolism, antioxidant status and intestinal microbiota. *Antioxidants* 12(12):2128
50. Hu W, Cao Y, Liu Q, Yuan C, Hu Z. 2024. Effect of salinity on the physiological response and transcriptome of spotted seabass (*Lateolabrax maculatus*). *Marine Pollution Bulletin* 203:116432
51. Mistry J, Chuguransky S, Williams L, Qureshi M, Salazar GA, et al. 2021. Pfam: the protein families database in 2021. *Nucleic Acids Research* 49(D1):D412–D419
52. Chen B, Li Y, Peng W, Zhou Z, Shi Y, et al. 2019. Chromosome-level assembly of the Chinese Seabass (*Lateolabrax maculatus*) genome. *Frontiers in Genetics* 10:275
53. Walker JM, ed. 2005. *The proteomics protocols handbook*. Totowa, NJ: Humana Press. doi: 10.1385/1592598900
54. Chou KC, Shen HB. 2010. Cell-PLoc 2.0: an improved package of web-servers for predicting subcellular localization of proteins in various organisms. *Natural Science* 2:1090–103
55. Tian Y, Wen H, Qi X, Zhang X, Liu S, et al. 2019. Characterization of full-length transcriptome sequences and splice variants of *Lateolabrax maculatus* by single-molecule long-read sequencing and their involvement in salinity regulation. *Frontiers in Genetics* 10:1126
56. Letunic I, Bork P. 2024. Interactive tree of life (iTOL) v6: recent updates to the phylogenetic tree display and annotation tool. *Nucleic Acids Research* 52(W1):W78–W82
57. Bailey TL, Johnson J, Grant CE, Noble WS. 2015. The MEME suite. *Nucleic Acids Research* 43(W1):W39–W49
58. Lu S, Wang J, Chitsaz F, Derbyshire MK, Geer RC, et al. 2020. CDD/SPARCLE: the conserved domain database in 2020. *Nucleic Acids Research* 48(D1):D265–D268
59. Waterhouse A, Bertoni M, Bienert S, Studer G, Tauriello G, et al. 2018. SWISS-MODEL: homology modelling of protein structures and complexes. *Nucleic Acids Research* 46(W1):W296–W303
60. Knuckles P, Carl SH, Musheev M, Niehrs C, Wenger A, et al. 2017. RNA fate determination through cotranscriptional adenosine methylation and microprocessor binding. *Nature Structural & Molecular Biology* 24:561–69
61. Gu Z. 2022. Complex heatmap visualization. *iMeta* 1(3):e43
62. Gu Z, Eils R, Schlesner M. 2016. Complex heatmaps reveal patterns and correlations in multidimensional genomic data. *Bioinformatics* 32(18):2847–49
63. Delaunay S, Helm M, Frye M. 2024. RNA modifications in physiology and disease: towards clinical applications. *Nature Reviews Genetics,* 25:104–22
64. Fan S, Xu X, Chen J, Yin Y, Zhao Y. 2024. Genome-wide identification, characterization, and expression analysis of m^{6}A readers-YTH domain-containing genes in alfalfa. *BMC Genomics* 25:18
65. Hazra D, Chapat C, Graille M. 2019. m^{6}A mRNA destiny: chained to the rhYTHm by the YTH-containing proteins. *Genes* 10(1):49
66. Sun J, Bie XM, Wang N, Zhang XS, Gao XQ. 2020. Genome-wide identification and expression analysis of YTH domain-containing RNA-binding protein family in common wheat. *BMC Plant Biology* 20:351
67. Geng S, Zheng W, Wang W, Lv X, Xin S, et al. 2023. The m^{6}A reader YTHDF2 modulates antiviral and antibacterial activity by suppressing METTL3 methylation-modified STING in fish. *The Journal of Immunology* 210(5):653–67
68. Zhang C, Guo C, Li Y, Ouyang L, Zhao Q, et al. 2021. The role of YTH domain containing 2 in epigenetic modification and immune infiltration of pan-cancer. *Journal of Cellular and Molecular Medicine* 25(18):8615–27
69. Liu Z, Wang T, She Y, Wu K, Gu S, et al. 2021. *N*^{6}-methyladenosine-modified circIGF2BP3 inhibits CD8$^+$ T-cell responses to facilitate tumor immune evasion by promoting the deubiquitination of PD-L1 in non-small cell lung cancer. *Molecular Cancer* 20:105
70. Wang Y, Xu L, Luo S, Sun X, Li J, et al. 2022. The m6A methylation profiles of immune cells in type 1 diabetes mellitus. *Frontiers in Immunology* 13:1030728
71. Zhou J, Wan J, Gao X, Zhang X, Jaffrey SR, et al. 2015. Dynamic m^{6}A mRNA methylation directs translational control of heat shock response. *Nature* 526:591–94